Chemistry – A European Journal

ChemEurJ Chemistry Europe European Chemical Societies Publishing

RESEARCH ARTICLE OPEN ACCESS

Synthesis of Tris(indol-3-yl)methanes From Indoles, CO_2, and Dimethylphenylsilane With BPh_3: Two-Step Construction of π-Conjugated Systems

Sha Li | So Saibara | Reito Yasui | Kazuto Takaishi | Natsumi Nitta | Tadashi Ema

Graduate School of Environmental, Life, Natural Science and Technology, Okayama University, Okayama, Japan

Correspondence: Natsumi Nitta (nitta@okayama-u.ac.jp) | Tadashi Ema (ema@cc.okayama-u.ac.jp)

Received: 4 April 2026 | **Revised:** 26 June 2026 | **Accepted:** 7 July 2026

Keywords: boranes | carbon dioxide fixation | cascade reaction | heteroaromatics | silanes

Tris(indol-3-yl)methanes were synthesized from indoles, CO_2, and $PhMe_2SiH$ in the presence of BPh_3 in acetonitrile at 50°C. This is the first CO_2 fixation reaction forming the aliphatic methine (>CH—) group. The isotope-labeling experiments clearly demonstrated that the carbon and hydrogen atoms of the methine group originated from carbon dioxide and dimethylphenylsilane, respectively. The mechanism for the multicomponent cascade reaction was elucidated by DFT calculations. One of the CO_2-derived products, tris(4-bromo-1-methylindol-3-yl)methane, underwent palladium-catalyzed intramolecular cascade reactions for the selective formation of two novel polycyclic heteroaromatic compounds, where the methine C(sp^3) atom originating from CO_2 was converted into aromatic C(sp^2) atoms. One is formally produced via double direct C—H arylation, Wacker-type oxidation, dehydrogenation, and debromination, while the other seems to be produced via the intramolecular homocoupling of aryl bromide, direct C—H arylation, Wacker-type oxidation, and dehydrogenation. Both of them are new intramolecular cascade reactions that are useful for the short-step construction of nitrogen-doped nanographenes. On the other hand, one of the CO_2-derived products, tris(1-pentylindol-3-yl)methane, was converted into tris(1-pentylindol-3-yl)methylium methanesulfonate, which is a potential antitumor drug. This is the first derivatization of CO_2 to a cationic C(sp^2) center.

1 | Introduction

Carbon dioxide (CO_2) is an abundant and renewable C1 resource that is increasingly important for sustainable organic synthesis [1–8]. Among various CO_2 fixation reactions, reductive CO_2 conversions play a key role in synthesizing value-added chemicals and have attracted much attention from chemists [9–14]. In particular, reductive CO_2 conversions with C—H/C—C bond formation have furnished valuable compounds such as aldehydes [15–21], alcohols [22–25], alkanes [26–29], alkenes [30], heterocycles [31–37], and aromatics [38–40]. Hydrogen (H_2) [41], hydroboranes (*B*–H) [42], and hydrosilanes (*Si*–H) [43–47] have been used as reductants, among which hydrosilanes show the advantage of moderate reactivity and stability in air. The catalytic hydrosilylation of CO_2 with hydrosilanes proceeds stepwise, generating silyl formates, bis(silyl)acetals, methoxysilanes, and methane, some of which are reactive intermediates (Scheme 1a) [48–52]. The hydrosilylation of CO_2 is thermodynamically favored because of the formation of the strong Si—O bonds.

Some derivatives of tris(1*H*-indol-3-yl)methanes such as turbomycin A and trisindoline are known as natural products (Figure S1) [53, 54], and others are known as drug candidates [55, 56] and chemosensors [57]. Tris(indol-3-yl)methanes can be synthesized by the electrophilic substitution reactions of the indole rings, and several carbon sources such as DMF and dimethyl carbonate can be used to construct the methine group [58–60]. However, there are no methods for the synthesis of

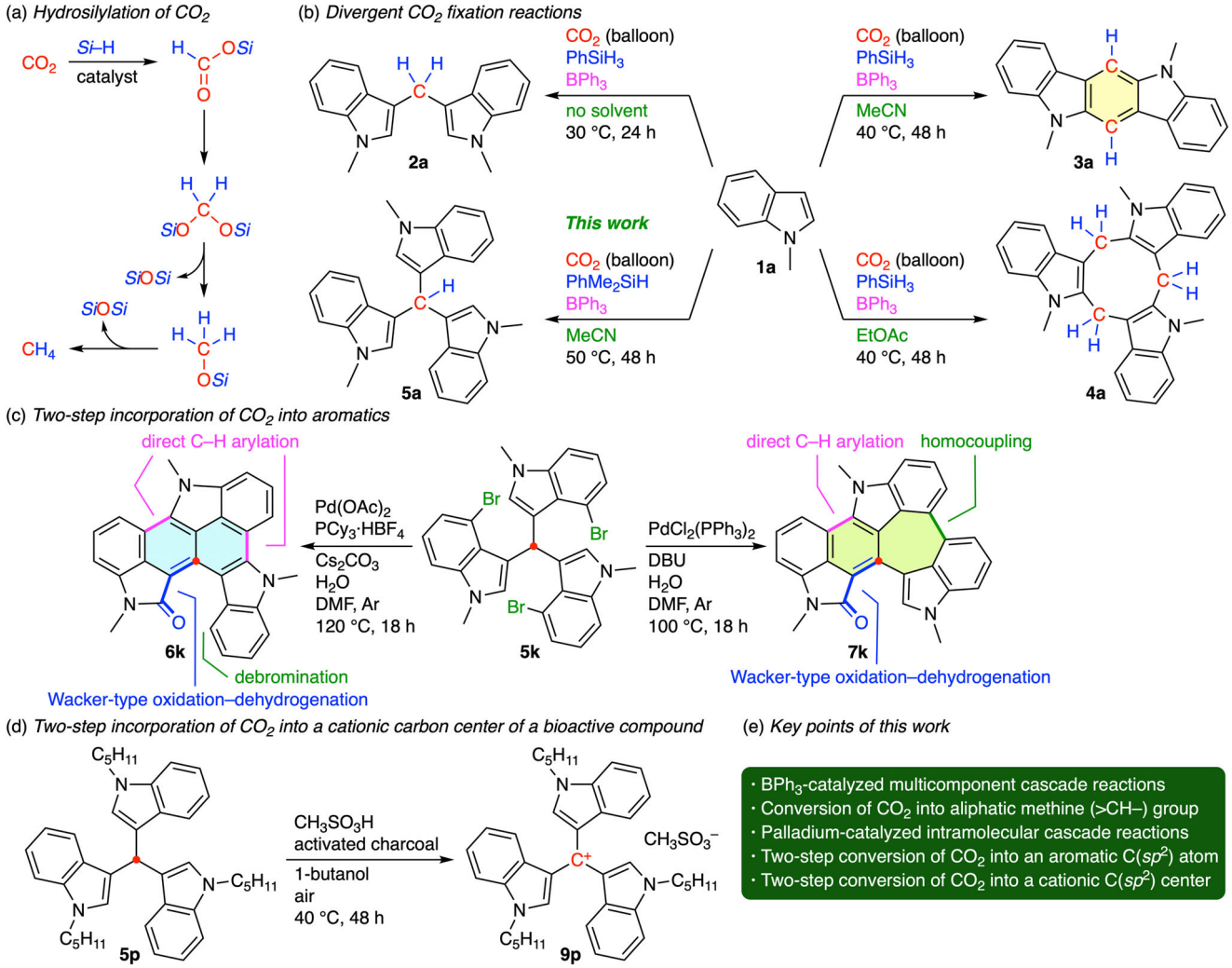

SCHEME 1 | (a) Stepwise CO_2 reduction with hydrosilane. (b) Diverse derivatizations of **1a** with CO_2. (c) Transformation of CO_2-derived **5k** into polycyclic heteroaromatic compounds **6k** and **7k**. (d) Transformation of CO_2-derived **5p** into biologically active compound **9p**. (e) Key points of this work.

tris(indol-3-yl)methanes from indoles and CO_2. On the other hand, further transformation of tris(indol-3-yl)methanes into other compounds is quite rare and unexploited despite the potentially useful synthetic platform with three indole rings disposed in proximity [61].

Previously, we synthesized diindolylmethane **2a** from 1-methylindole (**1a**), CO_2, and phenylsilane ($PhSiH_3$) using triphenylborane (BPh_3) as a catalyst under solvent-free conditions at 30°C (Scheme 1b) [62, 63]. The methylene bridge between the two aromatic rings was constructed from CO_2 and $PhSiH_3$. Recently, we achieved the selective synthesis of different carbocycles from indoles, CO_2, and $PhSiH_3$ in organic solvents at 40°C; indolo[3,2-*b*]carbazole **3a** was produced from two indoles and two CO_2 molecules in acetonitrile, while nine-membered cyclophane **4a** was constructed from three indoles and three CO_2 molecules in ethyl acetate [39]. Here, we report the synthesis of tris(1-methylindol-3-yl)methane (**5a**) from **1a**, CO_2, and dimethylphenylsilane ($PhMe_2SiH$) in acetonitrile at 50°C (Scheme 1b). This is the first example of the CO_2 conversion into the aliphatic methine (>CH—) group. Here we also report the two-step incorporation of CO_2 into functional π-conjugated compounds such as fluorescent polycyclic heteroaromatic compounds (Scheme 1c) and an anticancer drug candidate (Scheme 1d). The former is a new class of palladium-catalyzed intramolecular cascade reactions that are useful for the short-step construction of nitrogen-doped nanographenes, while the latter is the first derivatization of CO_2 to a cationic C(sp^2) center. The two-step protocols represent new and powerful ways of forming π-conjugated C(sp^2) atoms from CO_2.

2 | Results and Discussion

We noticed the formation of tris(1-methylindol-3-yl)methane (**5a**) when $PhMe_2SiH$ was used instead of $PhSiH_3$ under otherwise the standard reaction conditions for the synthesis of **3a** from **1a** in the presence of BPh_3 in acetonitrile at 40°C under CO_2 atmosphere (balloon) (Table 1, entry 1). It should be noted that the main product was completely switched from **3a** to **5a** by

TABLE 1 | Optimization of reaction conditions for **5a**.[a]

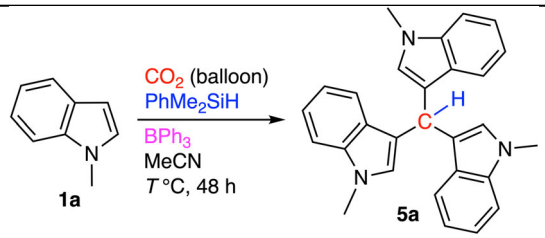

Entry	$PhMe_2SiH$ [mmol]	BPh_3 [mmol]	*T* [°C]	Yield [%][b]
1	1.8	0.25	40	75 (0)[c]
2	2.0	0.25	40	93
3	2.2	0.25	40	77
4	2.0	0.18	40	94
5	2.0	0.10	40	97
6	2.0	0.06	40	68
7	2.0	0.10	30	43
8	2.0	0.10	50	99 (98)[d]
9	2.0	0.10	60	91
10	2.0	0.10	70	79
11	2.0	0.10	50	0[e]
12	2.0	0.10	50	0[f]

[a]Reaction conditions: **1a** (1.0 mmol), CO_2 (balloon), $PhMe_2SiH$ (amount indicated above), BPh_3 (amount indicated above), MeCN (0.8 mL), 48 h.
[b]Determined by ^1H NMR spectroscopy using mesitylene as an internal standard.
[c]$PhMeSiH_2$, Ph_2SiH_2, Ph_2MeSiH, Ph_3SiH, Et_3SiH, $(EtO)_3SiH$, or PMHS was used instead of $PhMe_2SiH$.
[d]Isolated yield.
[e]In DMSO, DMF, EtOAc, toluene, THF, or under solvent-free conditions.
[f]$B(C_6F_5)_3$ instead of BPh_3. 1-Methylindoline was obtained in 45% yield.

simply changing the hydrosilane from $PhSiH_3$ to $PhMe_2SiH$. Interestingly, the screening of various hydrosilanes revealed that **5a** was produced only when $PhMe_2SiH$ was employed. The reaction conditions for **5a** were optimized as follows. The yield of **5a** was improved by setting the amount of $PhMe_2SiH$ to 2.0 mmol (entries 1–3). **5a** was obtained in 97% yield when the amount of BPh_3 was decreased to 5 mol% (based on $PhMe_2SiH$) (entries 2 and 4–6). The reaction temperature was also important, and the highest yield of 99% was attained at 50°C (entries 5 and 7–10). The reactions in other solvents or without solvent did not produce **5a** at all with a large amount of **1a** (73%–93%) recovered (entry 11). Because $PhMe_2SiH$ was well consumed in all the solvents except ethyl acetate, the electrophilic aromatic substitution reaction catalyzed by BPh_3 is considered to proceed only in acetonitrile, and the reactive species derived from $PhMe_2SiH$ and CO_2 seems to be much less reactive than those derived from $PhSiH_3$ and CO_2 [39, 62]. A control reaction using $B(C_6F_5)_3$ instead of BPh_3 under otherwise the optimized reaction conditions resulted in no formation of **5a**, but 1-methylindoline was obtained in 45% yield (entry 12) [39, 62].

The substrate scope was investigated under the optimized reaction conditions (Scheme 2). **5a** and **5b** having the methyl group at the 5-position were isolated in high yields (93%–98%), whereas **5c**–**f** having the halogen atom or the ester group at the 5-position were obtained in modest to good yields (41%–79%). Indoles **1g**–**i** with the electron-donating or electron-withdrawing group at the 6-position were converted into **5g**–**i** in high yields (81%–90%). These results indicate that the electron-rich indole rings are more reactive and beneficial for this reaction. **5j** was obtained in a modest yield (65%) as compared to **5b**, **5g**, and **5l** (90%–93%), which suggests the steric hindrance of the methyl group at the 4-position of **1j**. The lower yields of **5k** and **5m** are due to the bromine atom at the 4-position that caused steric and electron-withdrawing effects. The substituent on the nitrogen atom was modestly influential in reactivity; **5n**–**q** with the alkyl group were obtained in good to high yields (62%–84%), while **5r** with the phenyl group was obtained in a modest yield (51%) even with a catalyst loading of 10 mol%. When **1a** was allowed to react with $^{13}CO_2$ under otherwise the standard reaction conditions, **5a'** with the ^{13}C-labeled methine group was obtained in 97% yield. The ^1H and ^{13}C NMR spectra of **5a'** showed a doublet at 6.16 ppm ($^1J_{CH}$ = 124 Hz) and an intensified signal at 31.0 ppm, respectively, which indicates that the carbon atom of the methine group originated from carbon dioxide. The use of $PhMe_2SiD$ under otherwise the standard reaction conditions afforded **5a"** with the D-labeled methine group in 73% yield. The ^{13}C NMR spectrum of **5a"** showed a weak triplet signal at 30.8 ppm, which demonstrates that the hydrogen atom of the methine group originated from dimethylphenylsilane. The molecular structures

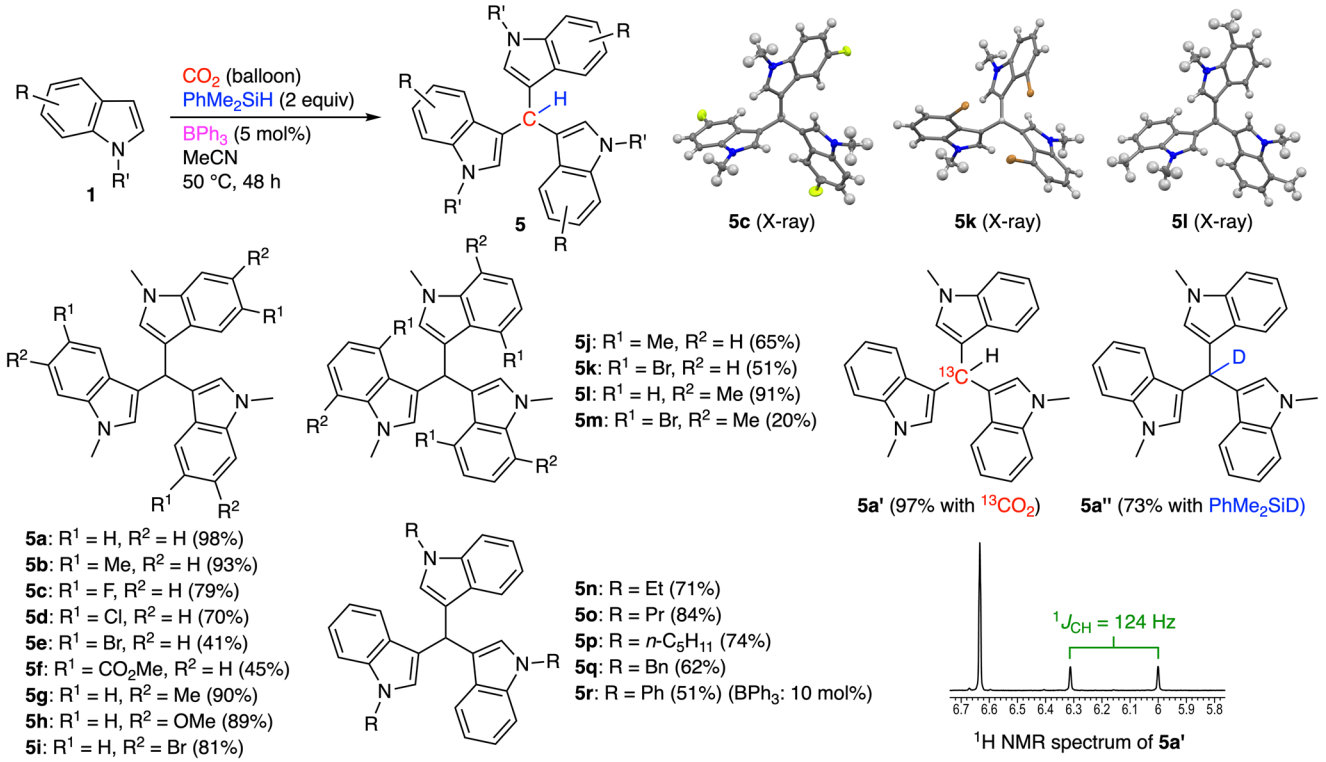

SCHEME 2 | Substrate scope and isotope labeling experiments. X-ray crystal structures of **5c**, **5k**, and **5l** (CCDC 2500296–2500298) are also shown.

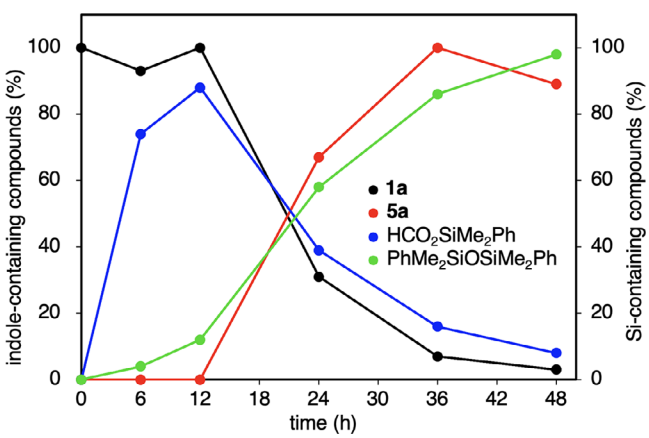

FIGURE 1 | Time course of the standard reaction of **1a**.

of **5c**, **5k**, and **5l** were unambiguously determined by X-ray crystallography.

To gain an insight into the reaction mechanism, we monitored the progress of the standard reaction of **1a** by means of ^{1}H NMR spectroscopy (Figures 1 and S2). $PhMe_2SiH$ was completely consumed in 6 h with the formation of silyl formate (HCO_2SiMe_2Ph), which reached the peak in 12 h without consuming **1a**. Subsequently, **1a** and HCO_2SiMe_2Ph were smoothly consumed to afford **5a** and disiloxane ($PhMe_2SiOSiMe_2Ph$), and no intermediates containing the indole ring were detected. The fact that HCO_2SiMe_2Ph was temporarily accumulated suggests that the reaction of **1a** with HCO_2SiMe_2Ph is the rate-determining step.

Several control experiments were conducted to address the reaction mechanism (Scheme 3). A 1:2 mixture of 3-formyl-1-methylindole and **1a** in acetonitrile was subjected to the BPh_3-catalyzed reaction under N_2 or CO_2 atmosphere, which resulted in no reactions (Scheme 3a,b). These results suggest that 3-formyl-1-methylindole cannot participate in the electrophilic substitution of **1a** even in the presence of BPh_3. When the same reaction under N_2 atmosphere was performed in the presence of $PhMe_2SiH$, only **2a** was detected (Scheme 3c). These results indicate that 3-formyl-1-methylindole is not an intermediate leading to the formation of **5a**. On the other hand, when a CO_2 hydrosilylation mixture was hydrolyzed, only formic acid was detected (66% yield), and neither formaldehyde nor methanol was detected (Scheme 3d and Figure S3), which suggests that HCO_2SiMe_2Ph is the reactive species. When **1a** was added to the solution containing HCO_2SiMe_2Ph and BPh_3 under N_2 atmosphere, the formation of **5a** was confirmed (Scheme 3e). These results strongly suggest that HCO_2SiMe_2Ph and BPh_3 act as a reactive intermediate and a catalyst, respectively. For comparison, HCO_2SiMe_2Ph was prepared by using tetrabutylammonium acetate (TBAA) as a catalyst (Figure S4), but this mixture showed no reactivity for **1a** (Scheme 3f), which demonstrates that BPh_3 is essential for the formation of **5a**. Control reactions without BPh_3, CO_2, or $PhMe_2SiH$ resulted in no formation of **5a**, indicating that all of them are essential for this CO_2 fixation reaction (data not shown).

We performed DFT calculations to clarify the reaction mechanism for the formation of **5a**. The energy profile, reaction path-

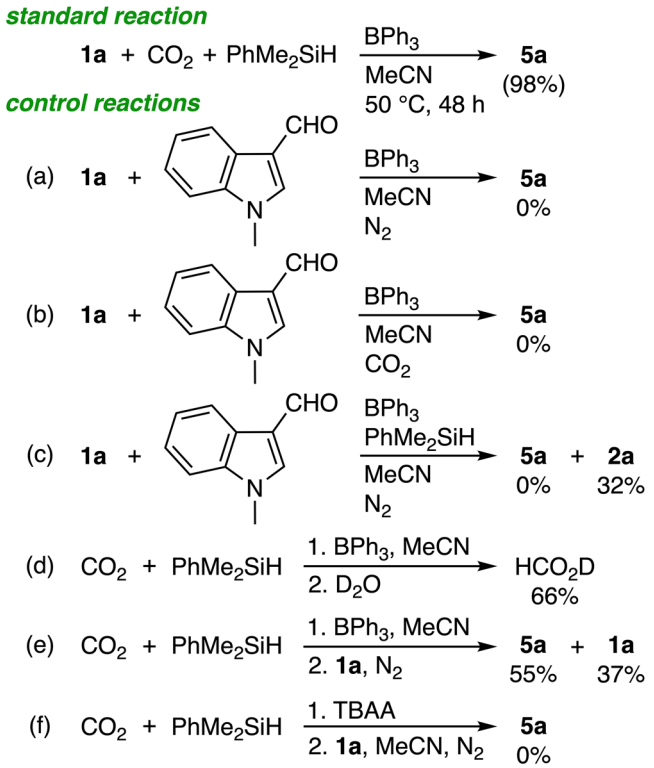

SCHEME 3 | Control experiments for the standard reaction of **1a**. Isolated yield in parenthesis (otherwise NMR yields).

way, and key transition-state structures are shown in Figure 2, and all the DFT-optimized structures are given in Figure S7. The electrophilic aromatic substitution of **1a** with HCO_2SiMe_2Ph activated by BPh_3 forms intermediate **I2** via **TS1** with a $\Delta G^{\ddagger}$ value of 23.5 kcal mol^{-1} and intramolecular proton transfer from the resulting Wheland intermediate (σ complex) **I1**. 1-Methyl-3-alkylidene-3*H*-indolium ion **I3** is generated via **TS2** by giving off $[HOBPh_3]^-$. The electrophilic addition of **I3** to **1a** furnishes **I4** via the highest-energy transition state **TS3**, and the subsequent proton abstraction affords **I5**. $[PhMe_2SiOBPh_3]^-$ leaves to generate indolium intermediate **I6** via **TS4** with a $\Delta G^{\ddagger}$ value of 23.6 kcal mol^{-1}. The electrophilic addition of **I6** to **1a** gives **I7** via **TS5**, and proton abstraction with $[PhMe_2SiOBPh_3]^-$ delivers **5a** and $PhMe_2SiOH$ with the regeneration of BPh_3. $PhMe_2SiOH$ is in equilibrium with $PhMe_2SiOSiMe_2Ph$ and water ($\Delta G_{calcd} = -3.4$ kcal mol^{-1}), the former of which was experimentally observed (Figure 1). We consider that the formation of $PhMe_2SiOSiMe_2Ph$ shifts the whole equilibrium to the right although the energy diagram suggests a reversible catalytic system. This reaction is also characterized by multiple rate-determining steps such as **TS1** and **TS4**. The fact that no indole-derived intermediates were detected during the time-course experiment (Figure 1) supports that **TS1** is the rate-determining step, and the multicomponent cascade reaction with multiple rate-determining steps can account for the dispersed accumulation of several reaction intermediates that are difficult to detect.

We explored the potential reactivity of tris(indol-3-yl)methanes **5**, taking advantage of the three indole rings juxtaposed in proximity. As a result, we found that **5k** could be converted into two novel polycyclic heteroaromatic compounds, **6k** and **7k**, which are constitutional isomers (Table 2). The molecular structures of **6k** and **7k** were unambiguously determined by X-ray crystallography. **6k** and **7k** have the uniquely fused ring systems, and the *P* and *M* enantiomers are present in the crystalline state, having slight nonplanarity and helical chirality induced by steric repulsion between the oxygen atom of the amide group and the hydrogen atom of the adjacent aromatic ring. We initially found that **6k** was obtained in 54% yield by the reaction of **5k** with $Pd(OAc)_2$, $PCy_3{\cdot}HBF_4$, and Cs_2CO_3 in DMF under Ar at 140°C for 18 h (entry 1). The reaction conditions for **6k** were then optimized as follows. Considering the possibility that a trace amount of water might serve as an oxygen source, we examined the effect of water on the reaction outcome, and the yield was increased to 65% in the presence of 100 equiv of water (entries 1–3). The use of *N*,*N*-dimethylacetamide (DMA) in place of DMF resulted in a lower yield (entry 4). The yield reached 75% at 120°C (entries 3, 5–7). PPh_3, PBu_3, and (*S*)-BINAP were almost comparable to PCy_3 (entries 6, 8–10). The reaction without the ligand gave **6k** in a moderate yield of 56% (entry 11). $Pd_2(dba)_3$ and $PdCl_2(PPh_3)_2$ were less productive (entries 12 and 13). We noticed the formation of a trace amount of **7k** when $PdCl_2(PPh_3)_2$ was used (entry 13). The reaction became less productive when K_2CO_3 or DBU was employed as a base, and a trace amount of **7k** was detected in the latter case (entries 14 and 15). We searched for reaction conditions suitable for the formation of **7k** (entries 16–18) and noticed that $PdCl_2(PPh_3)_2$ and DBU might be a good combination. In fact, increasing the amount of $PdCl_2(PPh_3)_2$ led to a significant enhancement in the outcome, and **7k** was obtained in 40% yield when 1 equiv of $PdCl_2(PPh_3)_2$ was used (entries 19–21). DMA resulted in a lower selectivity (entry 22). Finally, the impact of the reaction temperature was examined, and **7k** was obtained in the highest yield of 44% at 100°C (entries 23–25).

The selective cascade synthesis of **6k** or **7k** from **5k** poses fascinating mechanistic aspects. **6k** is formally constructed via double direct C—H arylation [64, 65], Wacker-type oxidation [66], dehydrogenation, and debromination, while **7k** seems to be constructed via homocoupling of aryl bromide, direct C—H arylation, Wacker-type oxidation, and dehydrogenation (Scheme 1c). To gain a mechanistic insight into the cascade reactions, we performed several control experiments (Scheme 4). Although the reaction was quenched in 1 h to identify intermediates, only **5k** and **6k** were detected in 25% and 16%, respectively, and no intermediates could be found (Scheme 4a). Cascade reactions driven by aromatization may proceed via different reaction pathways, or the first rate-determining reaction may be followed by low-barrier reactions. When bromine-free indole derivative **5a**, **2a**, or **1a** was used as a substrate under otherwise the standard reaction conditions for **6k**, Wacker-type oxidation did not proceed, and the substrates were recovered (Scheme 4b–d), which strongly suggests that Wacker-type oxidation takes place at a later stage in the synthesis of **6k** or **7k** from **5k**. In addition, 4-bromo-1-methylindole (**1k**) showed no reactivity, which suggests the importance of the intramolecular reaction (Scheme 4e). In contrast, when bromine-containing diindolylmethane **2k** was subjected to the same reaction conditions, **8k** was obtained in 78% yield (Scheme 4f), which is formally constructed via direct C—H arylation, Wacker-type oxidation, dehydrogenation, and debromination. The structure of **8k** was unambiguously

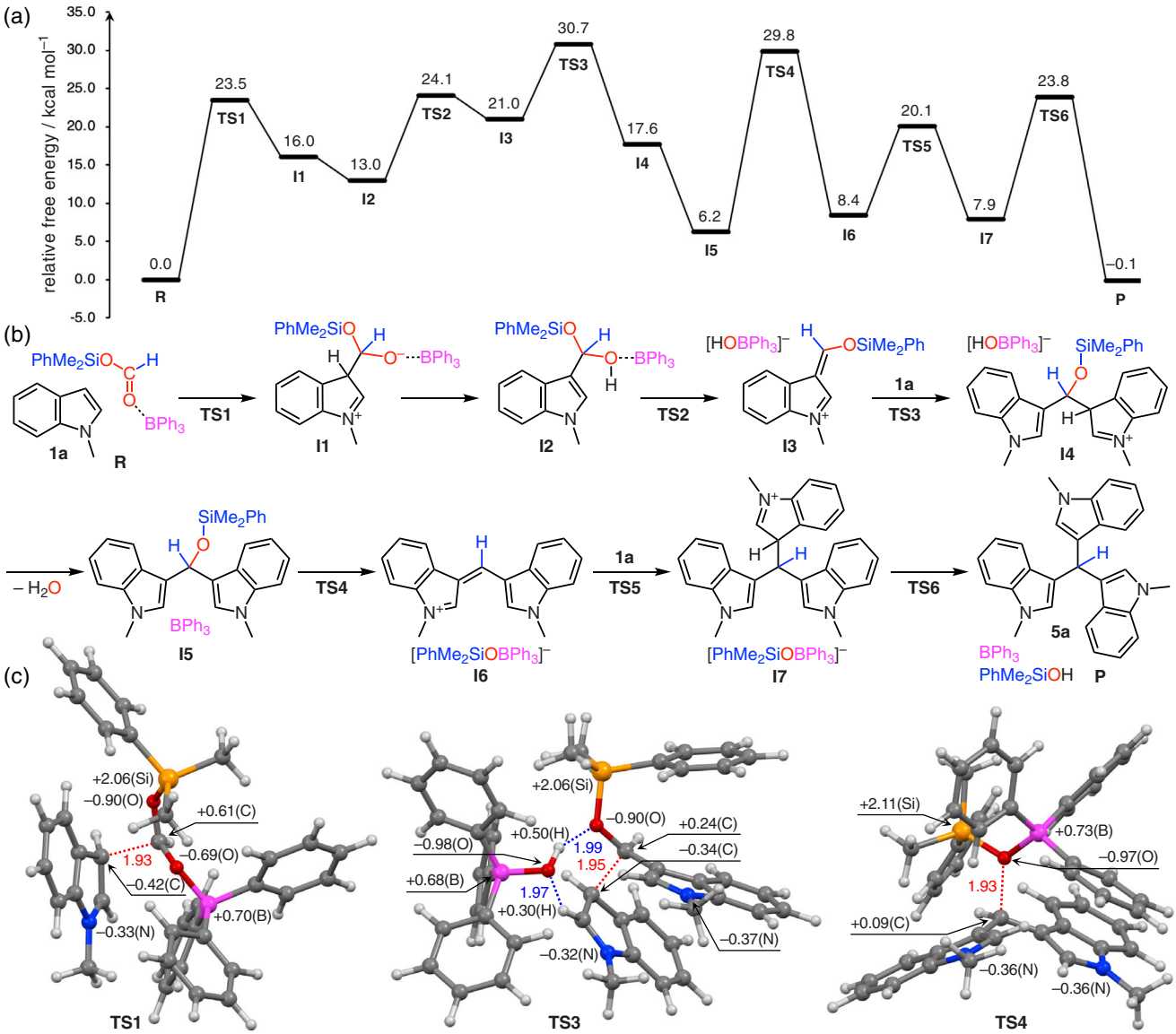

FIGURE 2 | (a) DFT-optimized free energy profile, where relative ΔG values at 323 K are shown in kcal mol^{-1}. DFT calculations were performed at the ωB97XD/6-31G(d) level of theory, and the self-consistent reaction field (SCRF) method with the polarizable continuum model (PCM) (acetonitrile) was adopted to take the solvation effect into account. (b) Reaction pathway. (c) Key transition-state structures, where distances (Å) are shown in blue and red, while natural bond orbital (NBO) charges are shown in black.

determined by X-ray crystallography. Based on these results, we consider that the intramolecular direct C—H arylation of **5k** is the initial reaction that triggers the cascade reaction leading to the formation of **6k**. On the other hand, the intramolecular homocoupling of aryl bromides of **5k** is likely to a determinant of the formation of **7k**. Apart from the mechanistic aspects, they are new and powerful synthetic methods for the construction of nitrogen-doped nanographenes.

We performed DFT calculations to characterize uniquely fused polycyclic heteroarenes **6k** and **7k** (Figure 3a,b). **6k** had a helicene-like geometry as observed for the crystal structure; the sum of the three dihedral angles of the inner rim of the [5]helicenoid moiety of **6k** was –27°. In contrast, **7k** had a slightly distorted planar geometry, and **7k** was 1.8 kcal mol^{-1} more stable than **6k**. Nucleus-independent chemical shifts (NICS) were calculated to gain insight into the local aromaticity of each ring in **6k** and **7k** [67], where NICS(0) was employed because the optimized structures of **6k** and **7k** were more or less nonplanar. The seven-membered ring in **7k** had antiaromaticity with a NICS(0) value of +10.91, which might be stabilized by the outer aromatic rings and the nitrogen atoms of the fused indole rings [68, 69]. Almost all the five- and six-membered rings except the lactam rings in **6k** and **7k** had good aromaticity, but only one hexagon in **6k** had poor aromaticity with a NICS(0) value of –2.51, which is reasonable if Clar's aromatic π-sextet rule is applied to **6k** (Figure S8) [70]. The photophysical properties of **6k** and **7k** were also studied. **6k** showed a few absorption bands in the UV region (250–380 nm) and weaker absorption bands in the visible region (380–480 nm) in CH_2Cl_2 and exhibited blue

TABLE 2 | Optimization of reaction conditions for the selective synthesis of **6k** or **7k**.[a]

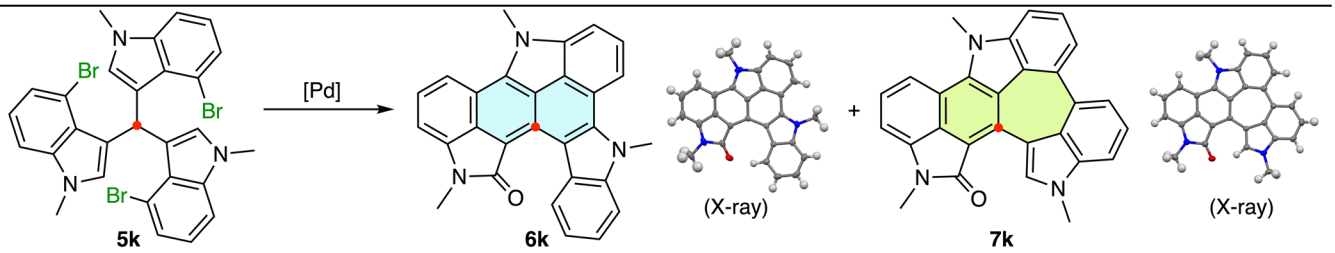

Entry	Catalyst	Ligand	Base	Solvent	T [°C]	Yield [%][b]	
						6k	7k
1[c]	$Pd(OAc)_2$	$PCy_3{\cdot}HBF_4$	Cs_2CO_3	DMF	140	54	0
2[d]	$Pd(OAc)_2$	$PCy_3{\cdot}HBF_4$	Cs_2CO_3	DMF	140	52	0
3	$Pd(OAc)_2$	$PCy_3{\cdot}HBF_4$	Cs_2CO_3	DMF	140	65	0
4	$Pd(OAc)_2$	$PCy_3{\cdot}HBF_4$	Cs_2CO_3	DMA	140	49	0
5	$Pd(OAc)_2$	$PCy_3{\cdot}HBF_4$	Cs_2CO_3	DMF	160	64	0
6	$Pd(OAc)_2$	$PCy_3{\cdot}HBF_4$	Cs_2CO_3	DMF	120	75 (76)	0
7	$Pd(OAc)_2$	$PCy_3{\cdot}HBF_4$	Cs_2CO_3	DMF	100	67	0
8	$Pd(OAc)_2$	PPh_3	Cs_2CO_3	DMF	120	73	0
9	$Pd(OAc)_2$	PBu_3	Cs_2CO_3	DMF	120	73	0
10	$Pd(OAc)_2$	(*S*)-BINAP	Cs_2CO_3	DMF	120	72	0
11	$Pd(OAc)_2$	—	Cs_2CO_3	DMF	120	56	0
12[e]	$Pd_2(dba)_3$	$PCy_3{\cdot}HBF_4$	Cs_2CO_3	DMF	120	73	0
13	$PdCl_2(PPh_3)_2$	$PCy_3{\cdot}HBF_4$	Cs_2CO_3	DMF	120	42	trace
14	$Pd(OAc)_2$	$PCy_3{\cdot}HBF_4$	K_2CO_3	DMF	120	59	0
15	$Pd(OAc)_2$	$PCy_3{\cdot}HBF_4$	DBU	DMF	120	37	trace
16	$PdCl_2(PPh_3)_2$	$PCy_3{\cdot}HBF_4$	DBU	DMF	120	22	trace
17	$PdCl_2(PPh_3)_2$	—	DBU	DMF	120	44	trace
18	$Pd(OAc)_2$	—	DBU	DMF	120	26	0
19[f]	$PdCl_2(PPh_3)_2$	—	DBU	DMF	120	31	11
20[g]	$PdCl_2(PPh_3)_2$	—	DBU	DMF	120	8	40
21[h]	$PdCl_2(PPh_3)_2$	—	DBU	DMF	120	5	32
22[g]	$PdCl_2(PPh_3)_2$	—	DBU	DMA	120	30	30
23[g]	$PdCl_2(PPh_3)_2$	—	DBU	DMF	100	8	44 (34)
24[g]	$PdCl_2(PPh_3)_2$	—	DBU	DMF	140	10	34
25[g]	$PdCl_2(PPh_3)_2$	—	DBU	DMF	80	12	32

[a]Reaction conditions: **5k** (30 μmol, 1 equiv), catalyst (6 μmol, 0.2 equiv), ligand (15 μmol, 0.5 equiv), base (210 μmol, 7 equiv), H_2O (3 mmol, 100 equiv), solvent (3 mL), Ar, 18 h. X-ray crystal structures of **6k** and **7k** (CCDC 2500299 and 2500300) are shown.
[b]Determined by ^1H NMR spectroscopy using mesitylene as an internal standard. Isolated yields in parentheses.
[c]H_2O (no addition).
[d]H_2O (30 μmol, 1 equiv).
[e]$Pd_2(dba)_3$ (3 μmol, 0.1 equiv).
[f]$PdCl_2(PPh_3)_2$ (15 μmol, 0.5 equiv).
[g]$PdCl_2(PPh_3)_2$ (30 μmol, 1 equiv).
[h]$PdCl_2(PPh_3)_2$ (45 μmol, 1.5 equiv).

fluorescence with two peaks at 477 nm and 505 nm (Figure 3c,d). **6k** had an absolute fluorescence quantum yield (Φ_F) of 38% and a fluorescence lifetime of 0.79 ns (Figure S5). On the other hand, **7k** showed several absorptions in the 250–500 nm region and exhibited green fluorescence with a peak at 503 nm (Figure 3c,d). **7k** had a Φ_F of 23% and a fluorescence lifetime of 1.30 ns (Figure S5).

Biologically active derivatives of tris(indol-3-yl)methanes are known. For example, tris(1-pentylindol-3-yl)methylium

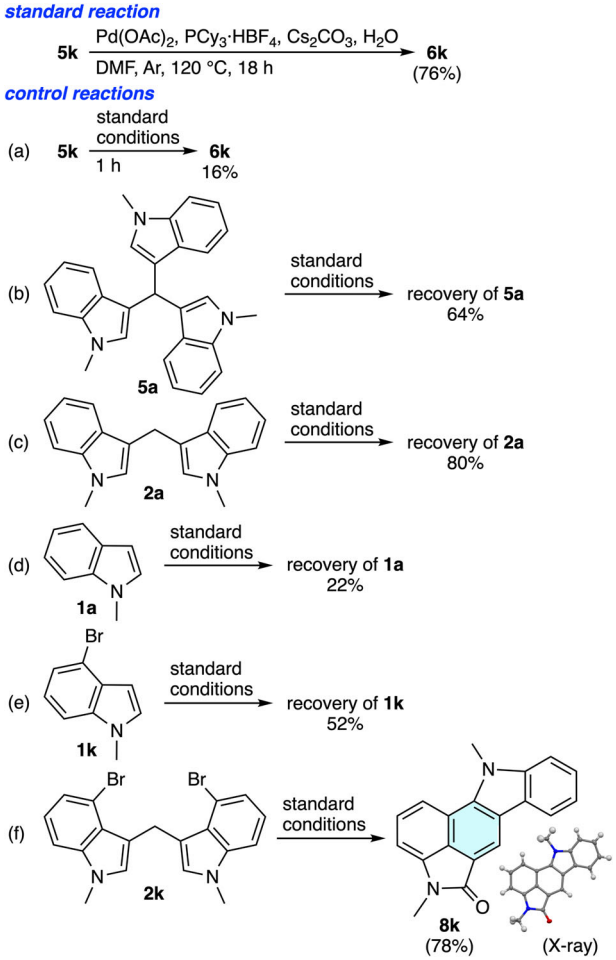

SCHEME 4 | Control experiments for the standard reaction of **5k**. Isolated yields in parentheses. X-ray crystal structure of **8k** (CCDC 2500301) is also shown.

methanesulfonate (**9p**) has exhibited higher cytotoxicity for human tumor cell lines such as HCT116 (colon cancer), K562 (leukemia), and Mel Kor (melanoma) than for normal cells of peripheral blood lymphocytes [55, 56]. We transformed CO_2-derived product **5p** to **9p** in 49% yield by air oxidation under acidic conditions (Scheme 1d). To the best of our knowledge, this is the first example of the derivatization of CO_2 into a cationic C(sp^2) center. Interestingly, **9p** showed a broad absorption band at 497 nm and fluorescence at 543 nm in toluene (Figure S6).

3 | Conclusion

Reductive conversions of CO_2 into divalent or trivalent groups such as the methylene and methine groups can lead to new and fascinating ways for the construction of the frameworks of organic compounds. Here, we have synthesized tris(indol-3-yl)methanes **5** from indoles **1**, CO_2, and $PhMe_2SiH$ using BPh_3 as a catalyst in acetonitrile. This is the first example of CO_2 fixation reactions forming the aliphatic methine (>CH—) group. Isotope-labeling experiments clearly demonstrated that the carbon and hydrogen atoms of the methine group originated from carbon dioxide and dimethylphenylsilane, respectively. DFT calculations indicated that the methine bridge between the three indole rings in **5** was formed by successive electrophilic aromatic substitution reactions, which was triggered by the reaction of **1** with the key reactive intermediate, HCO_2SiMe_2Ph. Novel polycyclic heteroaromatic compounds **6k** and **7k** were selectively synthesized from **5k** via the palladium-catalyzed intramolecular cascade reactions. X-ray crystallography and DFT calculations indicated that **6k** has a [5]helicenoid geometry, while **7k** contains an antiaromatic seven-membered ring. It should be noted that **6k** and **7k** were synthesized in just two steps from 4-bromo-1-methylindole (**1k**) and CO_2. This synthetic strategy may be applicable to the short-step synthesis of other polycyclic aromatics such as nitrogen-doped helicenes and nanographenes. Compound **9p** showing cytotoxicity for human tumor cell lines was also synthesized with CO_2 in two steps. The two-step protocols for the transformation of CO_2 into the π-conjugated C(sp^2) atom via the methine C(sp^3) atom are easy and sustainable methods for the synthesis of π-extended polycyclic heteroaromatic compounds.

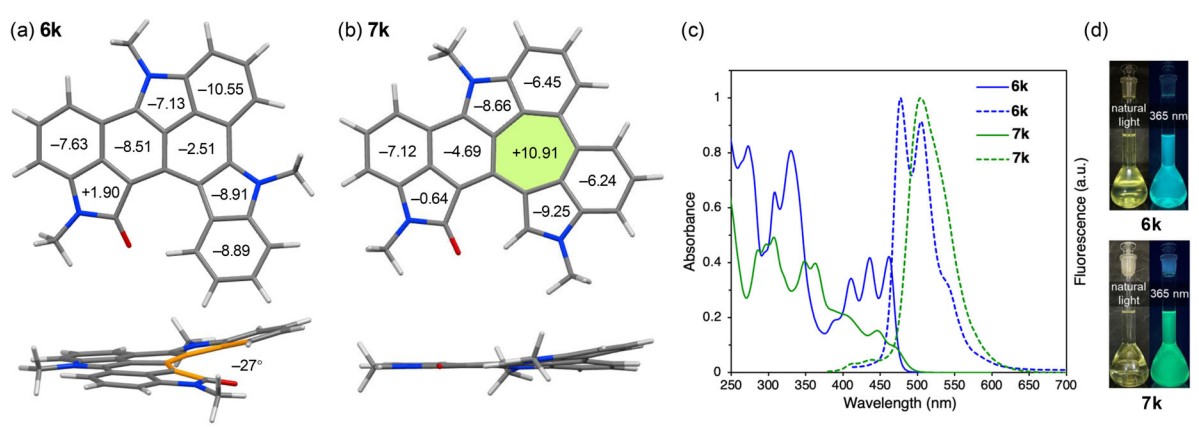

FIGURE 3 | (a, b) Top and side views of **6k** and **7k** optimized at the B3LYP/6-311+G(2d,p) level. NICS(0) values (in ppm) calculated at the GIAO-B3LYP/6-311+G(2d,p) level are indicated in the rings. The inner rim of the [5]helicenoid moiety of **6k** is shown in orange in the side view. (c) UV–vis absorption spectra (solid line) and fluorescence spectra (dotted line) of **6k** (2×10^{-5} M) in CH_2Cl_2 (λ_{ex} = 400 nm) and **7k** (2×10^{-5} M) in CH_2Cl_2 (λ_{ex} = 365 nm). (d) Photographs of solutions of **6k** and **7k**.

Acknowledgments

This work was supported by JSPS KAKENHI (Grant No. 20H02780 and 24K01488) and Okayama Foundation for Science and Technology. This work was also supported by JSPS Program for Forming Japan's Peak Research Universities (J-PEAKS) Grant No. JPJS00420230010. We thank Dr. Yukinari Sunatsuki (Okayama University) and Dr. Shigeki Mori (Ehime University) for X-ray analysis. We also thank Professor Eri Sakuda (Nagasaki University) for fluorescence lifetime measurements. We also thank Division of Instrumental Analysis, Okayama University for the measurements of NMR spectra. The computations were carried out at RCCS (Okazaki, Japan) (Project: 25-IMS-C098 and 26-IMS-C091).

Conflicts of Interest

The authors declare no conflicts of interest.

Data Availability Statement

The data that support the findings of this study are available in the Supporting Information of this article.

References

1. M. D. Burkart, N. Hazari, C. L. Tway, and E. L. Zeitler, "Opportunities and Challenges for Catalysis in Carbon Dioxide Utilization," *ACS Catalysis* 9 (2019): 7937–7956, https://doi.org/10.1021/acscatal.9b02113.

2. A. Dibenedetto and F. Nocito, "The Future of Carbon Dioxide Chemistry," *ChemSusChem* 13 (2020): 6219–6228, https://doi.org/10.1002/cssc.202002029.

3. D. A. Sable, K. S. Vadagaonkar, A. R. Kapdi, and B. M. Bhanage, "Carbon Dioxide Based Methodologies for the Synthesis of Fine Chemicals," *Organic & Biomolecular Chemistry* 19 (2021): 5725–5757, https://doi.org/10.1039/D1OB00755F.

4. T. Ema, "Selective Conversions of CO_2 Into Value-Added Chemicals via Cooperative Catalysis Using Multifunctional Catalysts," *Bulletin of the Chemical Society of Japan* 96 (2023): 693–701, https://doi.org/10.1246/bcsj.20230099.

5. Q.-W. Song, R. Ma, P. Liu, K. Zhang, and L.-N. He, "Recent Progress in CO_2 Conversion Into Organic Chemicals by Molecular Catalysis," *Green Chemistry* 25 (2023): 6538–6560, https://doi.org/10.1039/D3GC01892J.

6. R. Giovanelli, G. Bertuzzi, and M. Bandini, "Metal-Catalyzed Carbonylation Reactions With CO_2: An Update," *ChemCatChem* 15 (2023): e202300827, https://doi.org/10.1002/cctc.202300827.

7. M. N. Khan, Y. van Ingen, T. Boruah, A. McLauchlan, T. Wirth, and R. L. Melen, "Advances in CO_2 Activation by Frustrated Lewis Pairs: From Stoichiometric to Catalytic Reactions," *Chemical Science* 14 (2023): 13661–13695, https://doi.org/10.1039/D3SC03907B.

8. W. Natongchai, D. Crespy, and V. D'Elia, "CO_2 Fixation: Cycloaddition of CO_2 to Epoxides Using Practical Metal-Free Recyclable Catalysts," *Chemical Communications* 61 (2025): 419–440, https://doi.org/10.1039/D4CC05291A.

9. A. Tlili, E. Blondiaux, X. Frogneux, and T. Cantat, "Reductive Functionalization of CO_2 With Amines: An Entry to Formamide, Formamidine and Methylamine Derivatives," *Green Chemistry* 17 (2015): 157–168, https://doi.org/10.1039/C4GC01614A.

10. X.-F. Liu, X.-Y. Li, C. Qiao, and L.-N. He, "Transition-Metal-Free Catalysis for the Reductive Functionalization of CO_2 With Amines," *Synlett* 29 (2018): 548–555, https://doi.org/10.1055/s-0036-1591533.

11. X.-F. Liu, X.-Y. Li, and L.-N. He, "Transition Metal-Catalyzed Reductive Functionalization of CO_2," *European Journal of Organic Chemistry* 2019 (2019): 2437–2447, https://doi.org/10.1002/ejoc.201801833.

12. P. Sreejyothi and S. K. Mandal, "From CO_2 Activation to Catalytic Reduction: A Metal-Free Approach," *Chemical Science* 11 (2020): 10571–10593, https://doi.org/10.1039/d0sc03528a.

13. I. Dutta, S. S. Gholap, M. M. Rahman, et al., "Homogeneous Catalysis in *N*-Formylation/*N*-Methylation Utilizing Carbon Dioxide as the C1 Source," *Chemistry—An Asian Journal* 19 (2024): e202400497, https://doi.org/10.1002/asia.202400497.

14. S. Desmons, J. Bonin, M. Robert, and S. Bontemps, "Four-Electron Reduction of CO_2: From Formaldehyde and Acetal Synthesis to Complex Transformations," *Chemical Science* 15 (2024): 15023–15086, https://doi.org/10.1039/D4SC02888K.

15. X. Ren, Z. Zheng, L. Zhang, Z. Wang, C. Xia, and K. Ding, "Rhodium-Complex-Catalyzed Hydroformylation of Olefins With CO_2 and Hydrosilane," *Angewandte Chemie International Edition* 56 (2017): 310–313, https://doi.org/10.1002/anie.201608628.

16. Z. Liu, Z. Yang, B. Yu, et al., "Rhodium-Catalyzed Formylation of Aryl Halides With CO_2 and H_2," *Organic Letters* 20 (2018): 5130–5134, https://doi.org/10.1021/acs.orglett.8b02027.

17. T. Murata, M. Hiyoshi, M. Ratanasak, J. Hasegawa, and T. Ema, "Synthesis of Silyl Formates, Formamides, and Aldehydes via Solvent-Free Organocatalytic Hydrosilylation of CO_2," *Chemical Communications* 56 (2020): 5783–5786, https://doi.org/10.1039/D0CC01371D.

18. D. Li, L. Wei, W. Xiong, H. Jiang, and C. Qi, "Palladium-Catalyzed Reductive Formylation of Aryl Iodides With CO_2 Under Mild Conditions," *The Journal of Organic Chemistry* 88 (2023): 5231–5237, https://doi.org/10.1021/acs.joc.2c02576.

19. K. Nakaoka, C. Guo, Y. Saiki, S. Furukawa, and T. Ema, "Synthesis of Enamines, Aldehydes, and Nitriles From CO_2: Scope of the One-Pot Strategy via Formamides," *The Journal of Organic Chemistry* 88 (2023): 15444–15451, https://doi.org/10.1021/acs.joc.2c01666.

20. F. Yang, Y. Saiki, K. Nakaoka, and T. Ema, "One-Pot Synthesis of Aldehydes or Alcohols From CO_2 via Formamides or Silyl Formates," *Advanced Synthesis & Catalysis* 365 (2023): 877–883, https://doi.org/10.1002/adsc.202300031.

21. J. Sun, K. Zhao, H. Wang, and F. Shi, "Heterogeneous Bisphosphine Ligand-Encapsulated Rh Catalysts for Heterogeneous Hydroformylation of Alkenes With CO_2," *ACS Sustainable Chemistry & Engineering* 12 (2024): 12736–12743, https://doi.org/10.1021/acssuschemeng.4c01883.

22. Y. Tani, K. Kuga, T. Fujihara, J. Terao, and Y. Tsuji, "Copper-Catalyzed C–C Bond-Forming Transformation of CO_2 to Alcohol Oxidation Level: Selective Synthesis of Homoallylic Alcohols From Allenes, CO_2, and Hydrosilanes," *Chemical Communications* 51 (2015): 13020–13023, https://doi.org/10.1039/C5CC03932K.

23. X.-W. Chen, L. Zhu, Y.-Y. Gui, et al., "Highly Selective and Catalytic Generation of Acyclic Quaternary Carbon Stereocenters via Functionalization of 1,3-Dienes With CO_2," *Journal of the American Chemical Society* 141 (2019): 18825–18835, https://doi.org/10.1021/jacs.9b09721.

24. M.-Y. Wang, X. Jin, X. Wang, et al., "Copper-Catalyzed and Proton-Directed Selective Hydroxymethylation of Alkynes With CO_2," *Angewandte Chemie International Edition* 60 (2021): 3984–3988, https://doi.org/10.1002/anie.202012768.

25. D. Zhang, C. Jarava-Barrera, and S. Bontemps, "Selective Reductive Dimerization of CO_2 Into Glycolaldehyde," *ACS Catalysis* 11 (2021): 4568–4575, https://doi.org/10.1021/acscatal.1c00412.

26. K. Takaishi, H. Kosugi, R. Nishimura, Y. Yamada, and T. Ema, "*C*-Methylenation of Anilines and Indoles With CO_2 and Hydrosilanes Using a Pentanuclear Zinc Complex Catalyst," *Chemical Communications* 57 (2021): 8083–8086, https://doi.org/10.1039/D1CC03675K.

27. W. Xiong, X. Tan, H. Liu, et al., "Bimolecular Reduction of Carbon Dioxide: Double Synthons for Alkynes Trifunctionalization," *Science China Chemistry* 67 (2024): 841–847, https://doi.org/10.1007/s11426-023-1804-4.

28. Z. Guo, J. Wu, X. Wei, and C. Xi, "Selective *C*-Methylenation of *N*-Unsubstituted Indoles Using CO_2 Under $NaBH_4/I_2$ System," *ChemSusChem* 18 (2025): e202401491, https://doi.org/10.1002/cssc.202401491.

29. A. Kumar, R. Gupta, V. Subramaniyan, and G. Mani, "DMSO-Catalyzed CO_2 Reduction With 9-BBN: Selective Formation of Either Formoxy- or Methoxyborane Under Mild Conditions and *C*-Methylenation of Indoles," *Catalysis Science & Technology* 15 (2025): 678–688, https://doi.org/10.1039/D4CY01327A.

30. D.-Y. Zhu, W.-D. Li, C. Yang, J. Chen, and J.-B. Xia, "Transition-Metal-Free Reductive Deoxygenative Olefination With CO_2," *Organic Letters* 20 (2018): 3282–3285, https://doi.org/10.1021/acs.orglett.8b01155.

31. D.-Y. Zhu, L. Fang, H. Han, Y. Wang, and J.-B. Xia, "Reductive CO_2 Fixation via Tandem C−C and C−N Bond Formation: Synthesis of Spiro-indolepyrrolidines," *Organic Letters* 19 (2017): 4259–4262, https://doi.org/10.1021/acs.orglett.7b01906.

32. Y. Zhao, X. Guo, X. Ding, et al., "Reductive CO_2 Fixation via the Selective Formation of C−C Bonds: Bridging Enaminones and Synthesis of 1,4-Dihydropyridines," *Organic Letters* 22 (2020): 8326–8331, https://doi.org/10.1021/acs.orglett.0c02963.

33. Y. Zhao, X. Liu, L. Zheng, et al., "One-Pot Methylenation−Cyclization Employing Two Molecules of CO_2 With Arylamines and Enaminones," *The Journal of Organic Chemistry* 85 (2020): 912–923, https://doi.org/10.1021/acs.joc.9b02858.

34. W.-D. Li, J. Chen, D.-Y. Zhu, and J.-B. Xia, "Fe-Catalyzed Pictet-Spengler-Type Cyclization via Selective Four-Electron Reductive Functionalization of CO_2," *Chinese Journal of Chemistry* 39 (2021): 614–620, https://doi.org/10.1002/cjoc.202000521.

35. Z. Huang, Y. Li, J. Zhou, et al., "Palladium-Catalyzed Carbonylation for General Synthesis of Aurones Using CO_2," *ChemSusChem* 16 (2023): e202202365, https://doi.org/10.1002/cssc.202202365.

36. K. Takaishi, R. Nishimura, Y. Toda, H. Morishita, and T. Ema, "One-Pot Synthesis of Dihydropyrans via CO_2 Reduction and Domino Knoevenagel/Oxa-Diels−Alder Reactions," *Organic Letters* 25 (2023): 1370–1374, https://doi.org/10.1021/acs.orglett.3c00047.

37. K. Takaishi, H. Morishita, K. Iwaki, and T. Ema, "Deoxygenative Dual CO_2 Conversions: Methylenation and Switchable *N*-Formylation/*N*-Methylation of Tryptamines," *Green Chemistry* 27 (2025): 5359–5365, https://doi.org/10.1039/D5GC00942A.

38. S. Xiang, W. Fan, W. Zhang, Y. Li, S. Guo, and D. Huang, "Aqueous CO_2 Fixation: Construction of Pyridine Skeletons in Cooperation With Ammonium Cations," *Green Chemistry* 23 (2021): 7950–7955, https://doi.org/10.1039/D1GC02303A.

39. S. Li, S. Nakahara, T. Adachi, T. Murata, K. Takaishi, and T. Ema, "Skeletal Formation of Carbocycles With CO_2: Selective Synthesis of Indolo[3,2-*b*]carbazoles or Cyclophanes From Indoles, CO_2, and Phenylsilane," *Journal of the American Chemical Society* 146 (2024): 14935–14941, https://doi.org/10.1021/jacs.4c04097.

40. Q. Yan, J. Nan, R. Cao, et al., "Substrate-Controlled Divergent Reductive Cyclization of 2-Arylanilines Using CO_2 as a Switching Reagent," *Organic Letters* 27 (2025): 510–516, https://doi.org/10.1021/acs.orglett.4c04538.

41. W.-H. Wang, Y. Himeda, J. T. Muckerman, G. F. Manbeck, and E. Fujita, "CO_2 Hydrogenation to Formate and Methanol as an Alternative to Photo- and Electrochemical CO_2 Reduction," *Chemical Reviews* 115 (2015): 12936–12973, https://doi.org/10.1021/acs.chemrev.5b00197.

42. S. Bontemps, "Boron-Mediated Activation of Carbon Dioxide," *Coordination Chemistry Reviews* 308 (2016): 117–130, https://doi.org/10.1016/j.ccr.2015.06.003.

43. F. J. Fernández-Alvarez and L. A. Oro, "Homogeneous Catalytic Reduction of CO_2 With Silicon-Hydrides, State of the Art," *ChemCatChem* 10 (2018): 4783–4796, https://doi.org/10.1002/cctc.201800699.

44. R. A. Pramudita and K. Motokura, "Transformative Reduction of Carbon Dioxide Through Organocatalysis With Silanes," *Green Chemistry* 20 (2018): 4834–4843, https://doi.org/10.1039/C8GC02052C.

45. Y. Zhang, T. Zhang, and S. Das, "Catalytic Transformation of CO_2 Into C1 Chemicals Using Hydrosilanes as a Reducing Agent," *Green Chemistry* 22 (2020): 1800–1820, https://doi.org/10.1039/C9GC04342J.

46. Z. Li, Z. Yu, X. Luo, et al., "Recent Advances in Liquid Hydrosilane-Mediated Catalytic *N*-Formylation of Amines With CO_2," *RSC Advances* 10 (2020): 33972–34005, https://doi.org/10.1039/D0RA05858K.

47. R. A. Pramudita and K. Motokura, "Heterogeneous Organocatalysts for the Reduction of Carbon Dioxide With Silanes," *ChemSusChem* 14 (2021): 281–292, https://doi.org/10.1002/cssc.202002300.

48. D. Mukherjee, D. F. Sauer, A. Zanardi, and J. Okuda, "Selective Metal-Free Hydrosilylation of CO_2 Catalyzed by Triphenylborane in Highly Polar, Aprotic Solvents," *Chemistry—A European Journal* 22 (2016): 7730–7733, https://doi.org/10.1002/chem.201601006.

49. M. Rauch and G. Parkin, "Zinc and Magnesium Catalysts for the Hydrosilylation of Carbon Dioxide," *Journal of the American Chemical Society* 139 (2017): 18162–18165, https://doi.org/10.1021/jacs.7b10776.

50. M. Rauch, Z. Strater, and G. Parkin, "Selective Conversion of Carbon Dioxide to Formaldehyde via a Bis(silyl)acetal: Incorporation of Isotopically Labeled C_1 Moieties Derived From Carbon Dioxide Into Organic Molecules," *Journal of the American Chemical Society* 141 (2019): 17754–17762, https://doi.org/10.1021/jacs.9b08342.

51. H. H. Cramer, B. Chatterjee, T. Weyhermüller, C. Werlé, and W. Leitner, "Controlling the Product Platform of Carbon Dioxide Reduction: Adaptive Catalytic Hydrosilylation of CO_2 Using a Molecular Cobalt(II) Triazine Complex," *Angewandte Chemie International Edition* 59 (2020): 15674–15681, https://doi.org/10.1002/anie.202004463.

52. F. Ritter, T. P. Spaniol, I. Douair, L. Maron, and J. Okuda, "Molecular Zinc Hydride Cations $[ZnH]^+$: Synthesis, Structure, and CO_2 Hydrosilylation Catalysis," *Angewandte Chemie International Edition* 59 (2020): 23335–23342, https://doi.org/10.1002/anie.202011480.

53. M. Kobayashi, S. Aoki, K. Gato, K. Matsunami, M. Kurosu, and I. Kitagawa, "Marine Natural Products. XXXIV. Trisindoline, a New Antibiotic Indole Trimer, Produced by a Bacterium of *Vibrio* sp. Separated From the Marine Sponge *Hyrtios altum*," *Chemical and Pharmaceutical Bulletin* 42 (1994): 2449–2451, https://doi.org/10.1248/cpb.42.2449.

54. D. E. Gillespie, S. F. Brady, A. D. Bettermann, et al., "Isolation of Antibiotics Turbomycin A and B From a Metagenomic Library of Soil Microbial DNA," *Applied and Environmental Microbiology* 68 (2002): 4301–4306, https://doi.org/10.1128/AEM.68.9.4301-4306.2002.

55. S. N. Lavrenov, Y. N. Luzikov, E. E. Bykov, et al., "Synthesis and Cytotoxic Potency of Novel Tris(1-alkylindol-3-yl)methylium Salts: Role of *N*-Alkyl Substituents," *Bioorganic & Medicinal Chemistry* 18 (2010): 6905–6913, https://doi.org/10.1016/j.bmc.2010.07.025.

56. E. V. Stepanova, A. A. Shtil, S. N. Lavrenov, et al., "Tris(1-alkylindol-3-yl)methylium Salts as a Novel Class of Antitumor Agents," *Russian Chemical Bulletin* 59 (2010): 2259–2267, https://doi.org/10.1007/s11172-010-0386-7.

57. D. Sain, C. Kumari, A. Kumar, and S. Dey, "Indole-Based Distinctive Chemosensors for 'Naked-Eye' Detection of CN^- and HSO_4^-, Associated With Hydrogen-Bonded Complex and Their DFT Study," *Supramolecular Chemistry* 28 (2016): 239–248, https://doi.org/10.1080/10610278.2015.1092534.

58. M. Shiri, M. A. Zolfigol, H. G. Kruger, and Z. Tanbakouchian, "Bis- and Trisindolylmethanes (BIMs and TIMs)," *Chemical Reviews* 110 (2010): 2250–2293, https://doi.org/10.1021/cr900195a.

59. M. L. Deb, P. J. Borpatra, C. D. Pegu, R. Thakuria, P. J. Saikia, and P. K. Baruah, "Iodine/*tert*-Butyl Hydroperoxide-Mediated Reaction of Indoles With Dimethylformamide/Dimethylacetamide to Synthesize Bis- and Tris(indolyl)methanes," *ChemistrySelect* 2 (2017): 140–146, https://doi.org/10.1002/slct.201601857.

60. P. Nath, M. L. Deb, and P. K. Baruah, "Synthesis of Tris(indolyl)methanes by Using Dimethyl Carbonate as a Single Carbon Source via C-H Functionalization Approach," *Chemical Papers* 78 (2024): 1117–1124, https://doi.org/10.1007/s11696-023-03150-2.

61. M. T. El Sayed, K. M. Ahmed, K. Mahmoud, and A. Hilgeroth, "Synthesis, Cytostatic Evaluation and Structure Activity Relationships of Novel Bis-Indolylmethanes and Their Corresponding Tetrahydroindolocarbazoles," *European Journal of Medicinal Chemistry* 90 (2015): 845–859, https://doi.org/10.1016/j.ejmech.2014.12.008.

62. T. Murata, M. Hiyoshi, S. Maekawa, et al., "Deoxygenative CO_2 Conversions With Triphenylborane and Phenylsilane in the Presence of Secondary Amines or Nitrogen-Containing Aromatics," *Green Chemistry* 24 (2022): 2385–2390, https://doi.org/10.1039/D1GC04599G.

63. M. Ratanasak, T. Murata, T. Adachi, J. Hasegawa, and T. Ema, "Mechanism of BPh_3-Catalyzed *N*-Methylation of Amines With CO_2 and Phenylsilane: Cooperative Activation of Hydrosilanes," *Chemistry—A European Journal* 28 (2022): e202202210, https://doi.org/10.1002/chem.202202210.

64. G. Albano, A. Punzi, M. A. M. Capozzi, and G. M. Farinola, "Sustainable Protocols for Direct C–H Bond Arylation of (Hetero)Arenes," *Green Chemistry* 24 (2022): 1809–1894, https://doi.org/10.1039/D1GC03168F.

65. P. Yadav, N. Velmurugan, and C. K. Luscombe, "Recent Advances in Room-Temperature Direct C–H Arylation Methodologies," *Synthesis* 55 (2023): 1–26, https://doi.org/10.1016/j.ejmech.2014.12.008.

66. X.-Y. Zhou, X. Chen, and L.-G. Wang, "Palladium-Catalyzed Wacker-Type Oxidation of *N*-Boc Indoles Under Mild Conditions," *Synlett* 27 (2016): 2742–2746, https://doi.org/10.1055/s-0036-1588069.

67. P. V. R. Schleyer, C. Maerker, A. Dransfeld, H. Jiao, and N. J. R. V. E. Hommes, "Nucleus-Independent Chemical Shifts: A Simple and Efficient Aromaticity Probe," *Journal of the American Chemical Society* 118 (1996): 6317–6318, https://doi.org/10.1021/ja960582d.

68. K. Oki, M. Takase, S. Mori, and H. Uno, "Synthesis and Isolation of Antiaromatic Expanded Azacoronene via Intramolecular Vilsmeier-Type Reaction," *Journal of the American Chemical Society* 141 (2019): 16255–16259, https://doi.org/10.1021/jacs.9b09260.

69. R. Dash, S. Maddala, P. Chetti, and V. Parthasarathy, "Benzo-Extended Thiaquasi[7]circulenes: Strategic Scholl-Type Synthesis, Tunable Electronic, and Stimuli-Responsive Properties," *Chemistry—A European Journal* 31 (2025): e202501471, https://doi.org/10.1002/chem.202501471.

70. M. Solà, "Forty Years of Clar's Aromatic π-Sextet Rule," *Frontiers in Chemistry* 1 (2013): 22, https://doi.org/10.3389/fchem.2013.00022.

Supporting Information

Additional supporting information can be found online in the Supporting Information section.

Experimental procedures, compound data, and DFT calculations. CCDC 2500296–2500301 contain the supplementary crystallographic data for this paper.

Supporting File 1: chem71464-sup-0001-SuppMat.pdf